AIAA JOURNAL
Vol. 43, No. 11, November 2005

Experimental Study on Capillary Flow in a Vane–Wall Gap Geometry

Yongkang Chen* and Steven H. Collicott†
Purdue University, West Lafayette, Indiana 47907-2023

Capillary flow in microgravity in the vane–wall gap geometry in a cylindrical container is studied experimentally. The flow is of interest because it affects the performance of vane-type propellant management devices, in which the vane–wall gap geometry is common. Different flow regimes, previously reported for the capillary flow in cylinders of various cross-section geometries, are identified using the data obtained in the Purdue University 1.2-s drop tower. Effects of geometric parameters, contact angle, and liquid viscosity on the flow are studied, with emphasis on the Lucas–Washburn flow regime. It is found that increases in gap size, liquid viscosity, contact angle, and vane edge bluntness decrease the capillary advance rate, while increases in the vane thickness and the vane obliquity angle enhance the capillary advance. In addition, some effort is made to gain insight into the interface profile with an approximate description.

Nomenclature

a = exponent of power law relation between L and t
L = meniscus tip location, mm
m = slope of least-squares line, mm/s$^{1/2}$
t = time, second
Z = interface minimum height, mm
α = vane obliquity angle, deg
γ = liquid contact angle, deg
δ = gap size, mm
ϵ = vane thickness, mm
σ = surface tension, N/m
ν = kinematic viscosity, cSt
ρ = liquid density, kg/m^3

Introduction

THE existence of equilibrium capillary surfaces in zero gravity in the vane–wall gap geometry in a cylindrical container, characterized by the critical contact angle or gap size, has been investigated in two previous studies.[1,2] Finite-height, single-valued equilibrium capillary surfaces fail to exist for all cases where the relevant parameters are subcritical. This nonexistence of the equilibrium surfaces is related to the occurrence of capillary-driven flows in the same geometry. That is, when constrained by either gravity or certain inertial forces, fluids in the cylindrical container under study always have equilibrium shapes; once the constraint forces disappear, given subcritical geometrical parameters, the fluid will wick up part of the container wall around the gap region to form a capillary-driven flow. Given sufficient time another equilibrium state will be reached in a finite-volume container, but not during the short-duration flows described in this paper. Historically, capillary-driven flow has been studied in a variety of geometries, such as interior corners[3] and rounded corners in "bathtubs."[4] Note that the capillary-driven flow defined earlier is different from interface reorientation, which is also driven by capillary forces in similar situations; an example can be found in Weislogel and Ross.[5]

The properties of the capillary flow in the vane–wall gap geometry concern the performance of the vane-type propellant management device (PMD), in which this geometry is common.[6] Improved understanding of this type of flow can help to improve the design of vane-type PMDs for liquid propellant systems or other similar surface-tension devices in weightlessness.

Capillary-driven flow in cylindrical containers of different cross-section geometry has long been studied for its importance in both fundamental and applied geometries. Most recently, an extensive study of the capillary rise flow in circular cylinders was performed by Stange et al.[7] Typical flow regimes have been identified with the aid of analytical and experimental results. Weislogel and Lichter[3] have studied the flow in interior corners, which are typical in containers of polygonal cross section. The capillary flow in rounded corners has been addressed by Ransohoff and Radke[8] and Dong and Chatzis.[9] Dreyer et al.[10,11] have studied the fluid motion in capillary vanes, which consist of two parallel plates mounted in a reservoir with a certain gap. Typically, it was found that the flow stops when the aspect ratio of the gap, i.e., the gap normalized by the width, is greater than unity.

The vane–wall gap geometry is a combination of two corners and a gap, as shown in Fig. 1. The presence of the gap changes the interface structure near the meniscus tip. This study addresses how this change in the meniscus tip structure affects the capillary flow as compared to flow in perfect corners, as in the case of zero gap. An analytical Lucas–Washburn type limiting-flow solution is attempted but is hindered by the complexity of the geometry, especially the curved cylindrical wall. This paper presents experimental results obtained with the Purdue drop tower. The flow regimes that the meniscus tip runs through during the capillary rise flow will be analyzed. Effects of geometric parameters, contact angle, and the fluid viscosity on the flow will be studied. In addition, the development of the interface profile will be addressed with some typical features extracted from the image data.

Experimental Setup

The experiments were conducted at Purdue University drop tower in the Aerospace Sciences Laboratory of the School of Aeronautics and Astronautics.[12] This facility provides 1.27 s of free fall with the g-residual estimated at $5 \times 10^{-5}\, g_0$ ($g_0 = 9.8$ m/s^2) (Ref. 13).

The test cell for these experiments is shown in Fig. 2. The acrylic cylinder in the center part is a fluid cell with a thin stainless-steel vane mounted near the cylinder wall. The cross-sectional geometry of the fluid cell is shown in Fig. 3. The distance DO′, measured perpendicular to the vane edge ST, is defined as the gap size and

Presented as Paper 2004-1149 at the AIAA 42nd Aerospace Sciences Meeting, Reno, NV, 5–8 January 2004; received 7 August 2004; revision received 19 January 2005; accepted for publication 3 May 2005.

*Postdoctoral Fellow, School of Aeronautics and Astronautics; currently Postdoctoral Fellow, P.O. Box 751-ME, Mechanical and Materials Engineering Department, Portland State University, Portland, OR 97207-0751. Member AIAA.

†Associate Professor, School of Aeronautics and Astronautics. Associate Fellow AIAA.

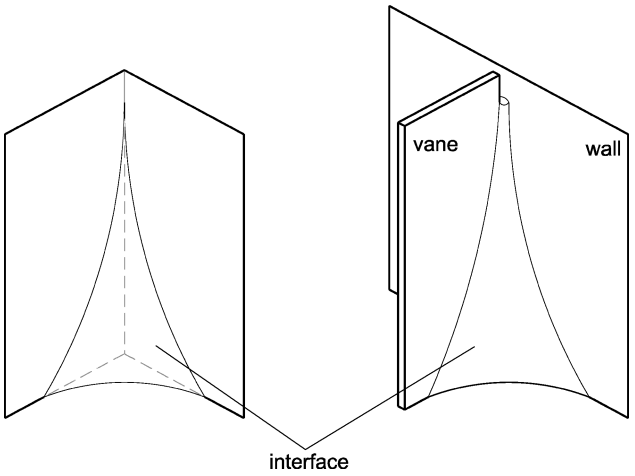

Fig. 1 Sketch of capillary menisci in an interior corner (left) and a vane–wall gap geometry (right).

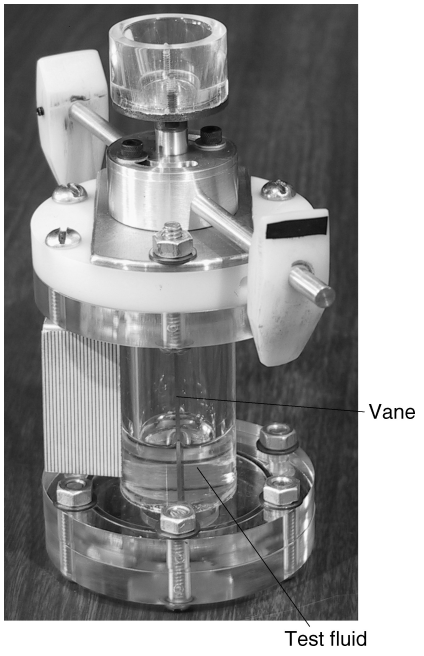

Fig. 2 Test cell.

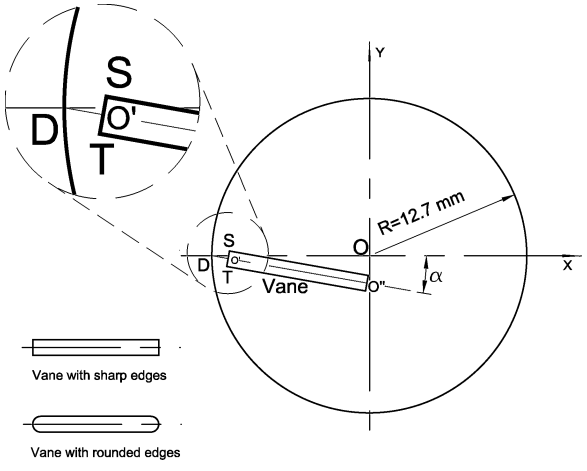

Fig. 3 Sketch of the cross section of the test cell.

Table 1 Parameters of the cylinder cross section

Variable	Value
Inner radius of cell r, mm	12.7
Vane thickness ϵ, mm	0.25, 0.51, 1.27, 2.54
Gap size δ, mm	0, 0.64, 1.27, 2.54
α, deg	0, 5, 10, 15, 20

Table 2 Relevant fluid and interfacial properties

Liquid	ν, cST	ρ, kg/m^3	σ, N/m	γ, deg
Silicon oil	2.0	872	0.0187	0
Silicon oil	5.0	913	0.0197	0
Silicon oil	20.0	949	0.0206	0
Eth/H_2O 30/70(%vol)	2.36	937	0.0364	51
Eth/H_2O 50/50(%vol)	2.75	896	0.0308	35
Eth/H_2O 70/30(%vol)	2.47	854	0.0275	15

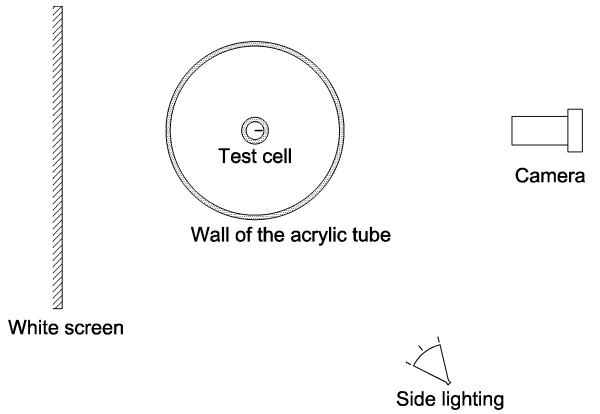

Fig. 4 Imaging geometry.

denoted as δ. The thickness of the vane ST is denoted as ϵ. The obliquity angle α is formed between centerline of the vane and the x axis by rotating the vane about D. The ranges of the geometric parameters examined in this study are listed in Table 1.

Images were obtained with a charge-coupled device camera falling outside of and parallel to the tower simultaneously with the test cell. A schematic of the imaging setup is given in Fig. 4. The drag forces on the falling camera package slow its motion slightly. Therefore at a certain moment the test cell falls out of the camera view. The data of one drop test could not cover the whole range, i.e., 1.27 s of free fall. For the data shown later, the data from 0 to about 0.9 s were acquired from one drop and the rest are acquired from several different drops by staggering the release of the test cell and the camera. This introduces some error into the results when the data are combined to generate a full data set.

A procedure for cleaning the test cell inner surface and the vane surface is followed strictly before each test to ensure repeatable surface quality. All test cell parts including the vane are first washed with warm soapy water and rinsed with distilled water. They are then rinsed in ethanol. In the end, distilled water is again used to rinse all the pieces, which are left to air-dry afterward. Silicon oil (polydimethylsiloxane, PDMS) of different viscosities was used as the primary test liquid. Additionally, mixtures of ethanol and distilled water with various concentration were used to create different contact angles. Physical properties of these liquid solutions are adopted from Weislogel and Ross[5] and listed in Table 2. The initial fill depth of the liquid in the test cell is 29.6 mm. This appears to be sufficiently deep not to affect the capillary rise in these tests.

Results and Discussion

Sequences of images were acquired and some examples are shown in Fig. 5. The liquid is driven by capillary forces and rises in the gap region, forming a slender column. The meniscus tip location, interface minimum, and interface profile are extracted from the images and discussed next.

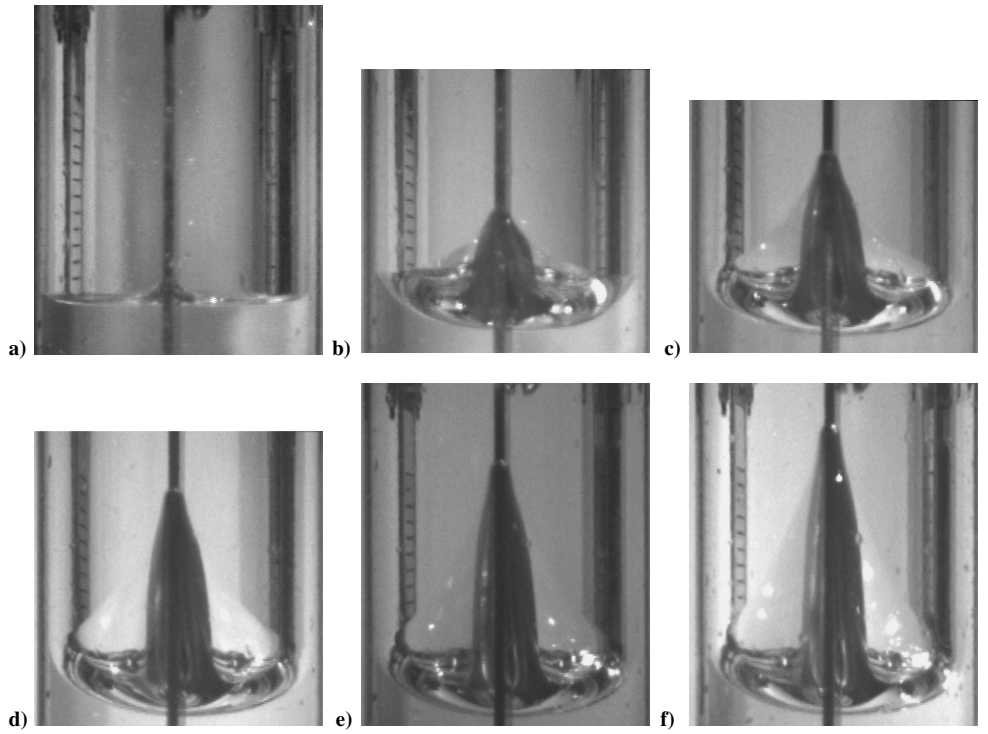

Fig. 5 Capillary rise in the vane–wall gap geometry in a circular cylindrical container; vane thickness ϵ, 1.27 mm; gap size δ, 0.64 mm: t = a) 0, b) 0.2, c) 0.4, d) 0.6, e) 0.8, and f) 1.0 s.

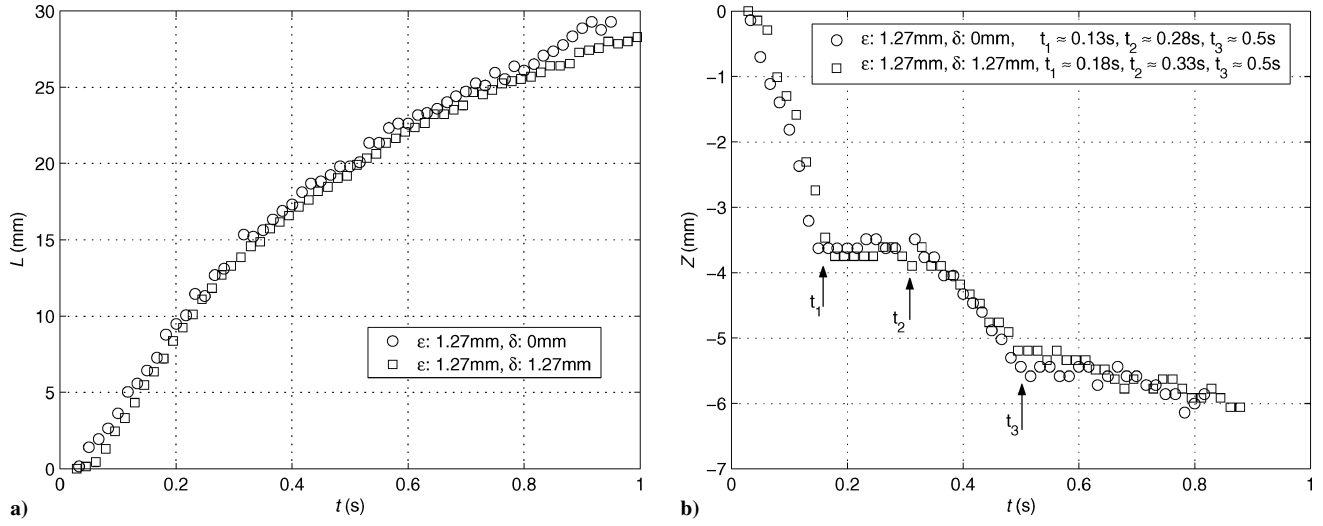

Fig. 6 Typical results from the capillary flow in the vane–wall gap geometry: a) meniscus tip location L as a function of t and b) interface minimum Z as a function of t.

Meniscus Tip Location and Interface Minimum

Two important features of the capillary-driven flow in a cylindrical container were measured: the distance traveled by the meniscus tip (or tip location) L, measured from the initial tip location, and the interface minimum Z, measured from the initial 1-g interface level. Although this study is focused on the flow in the corners connected by a gap, results for zero-gap cases are also included for comparison. Data of two typical cases are shown in Fig. 6.

According to Stange et al.,[7] capillary rise flow in cylindrical containers runs through several regimes. In each regime, the flow is dominated by the capillary driving forces exceeding a certain force working against them. In the first regime, there is competition between the inertial forces and the capillary forces, and the increase of the meniscus tip location L is proportional to t^2. In the second regime, there is convective pressure loss against the capillary forces, and consequently $L \sim t$. In the third or so-called Lucas–Washburn regime, the flow is governed by competition between viscous and capillary forces, leading to $L \sim t^{1/2}$. Furthermore, for the capillary flow in the interior corners, Weislogel and Lichter[3] pointed out that even in the Lucas–Washburn regime, the flow was observed as a constant flow with $L \sim t^{3/5}$ followed by a flow with $L \sim t^{1/2}$. In the $L \sim t^{1/2}$ regime, it is found that one point on the profile of the interface in its symmetry plane remains at a constant distance from the vertex of the corner. Such a regime is called "constant-height flow" according to Weislogel and Lichter.[3] Note that the height refers to a transverse distance instead of a streamwise one.

At the moment, the lack of a theoretical model of the flow in the vane–wall gap geometry makes it difficult to predict those flow regimes. For instance, even a proper length scale R could not easily be found to evaluate the inertial time scale $t_r = 0.413(\rho R^3/\sigma)^{1/2}$, as proposed by Siegert et al.[14]

It is easier to evaluate the range of the flow regimes by plotting the time history of the tip location L in log–log form, as shown in Fig. 7. The data shown here are one of the data sets shown in

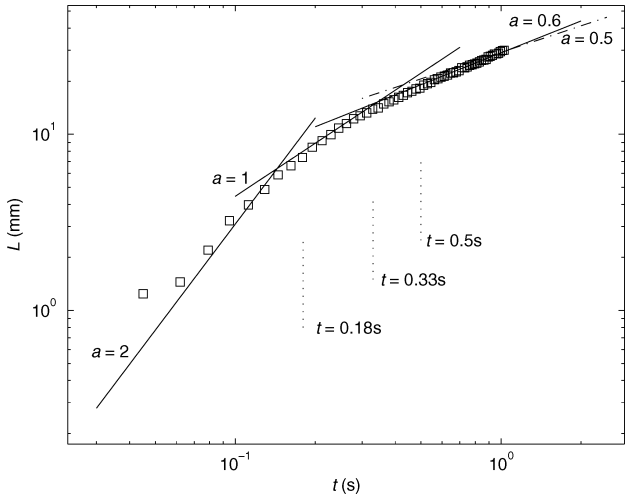

Fig. 7 Identification of flow regimes, with $L \sim t^a$, $\epsilon = 1.27$ mm, $\delta = 1.27$ mm.

Fig. 6a. Straight lines of different slopes a are drawn to help identify the likely range of each flow regime. The data positively show the existence of three flow regimes described in the precedings the inertial, convective, and constant-flow regimes. The data also show that the constant height flow regime might start in the late stage. For the inertial regime, the first couple of data points are off the line. This might be caused by both the error in data reduction and the dynamic contact-angle effect due to relatively large tip velocity at the beginning of the flow.

In the same figure, the three time locations marked with t_1 through t_3 are adopted from the interface minimum data shown in Fig. 6b, in which one can notice three clear turning points in the variation of the data. It is unclear whether there is a direct connection between these turning points and the divisions between different flow regimes.

Generally, the last regime, with $L \sim t^{1/2}$, represents a well-developed flow and is of most interest. Consequently, for all the meniscus tip location data shown below, interest is focused on this regime by plotting the tip location L or interface minimum Z vs $t^{1/2}$. The slope m of the least-squares fitted line in this region reveals the rate of the tip rise. Note that due to the experimental setup, as mentioned, the slope m is obtained by a linear least-squares fit to the data from a single drop. The time range for the least-squares calculations starts at $t = 0.4$ s and ends at large time, where the data end.

Effect of the Gap with the Vane Normal to the Wall

Figure 8 shows the effect of the gap size on the flow. It shows that m varies nonlinearly with gap size. Note that with δ increasing from 0 to 0.64 mm there is a slight increase of m, but it decreases for larger gaps. The capillary flow becomes extremely slow when δ approaches the critical value calculated by Chen and Collicott.[1]

For the zero-gap case, m can also be estimated by using the result of Weislogel and Lichter,[3]

$$L = 1.702 G^{\frac{1}{2}} H^{\frac{1}{2}} t^{\frac{1}{2}} \tag{1}$$

where G is determined by the flow cross-section geometry and the fluid properties, and H is the constant transverse "height" of the interface. H is calculated following the methods described by de Lazzer et al.[15] or Finn and Neel.[16] Figure 9 shows the location of the extremal arc Γ_0, which features the C-singular solution surface (details of computation can be found in Chen[13]). With the known radius of the arc Γ_0, H is obtained by subtracting R_0 from the distance O_1S. In the same fashion, H is also obtained for the non-zero-gap cases.

This is an approximate treatment because Eq. (1) is for corners formed with two planar walls, whereas in this study one of two walls is a section of a circular arc. In spite of the significant difference at large gap size, the results are presented in hopes that they may be useful for relatively small gap cases. Note that the m calculated by Eq. (1) is 5.5% less than the experimental value for the

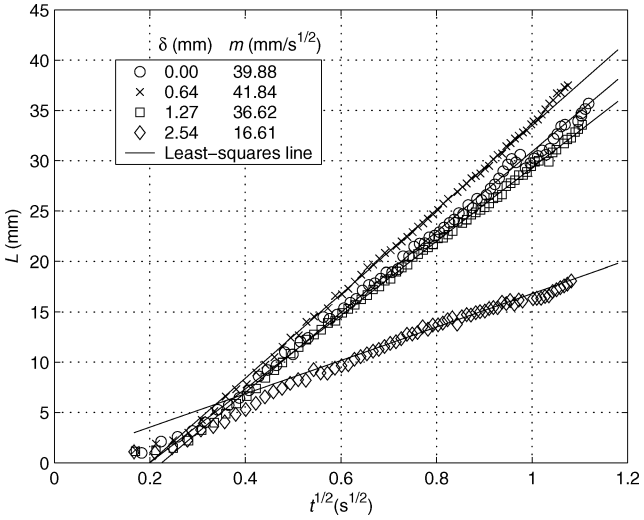

a)

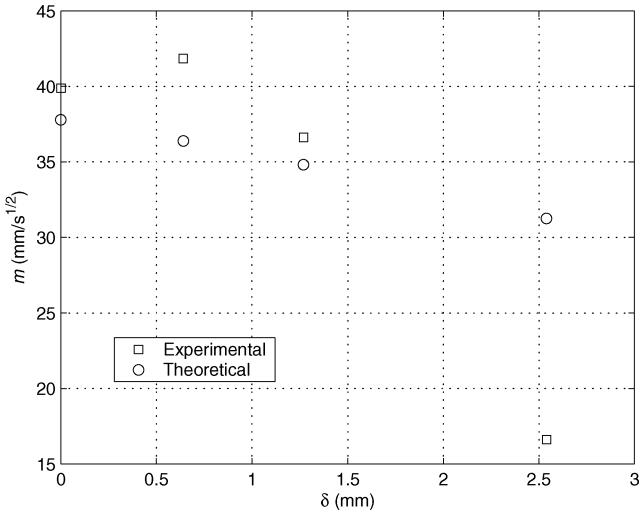

b)

Fig. 8 Capillary rise results with the vane normal to the wall, $\epsilon = 1.27$ mm, $\nu = 5$ cSt: a) meniscus tip location L as a function of $t^{1/2}$ and b) slope of $L \sim t^{1/2}$ flow regime.

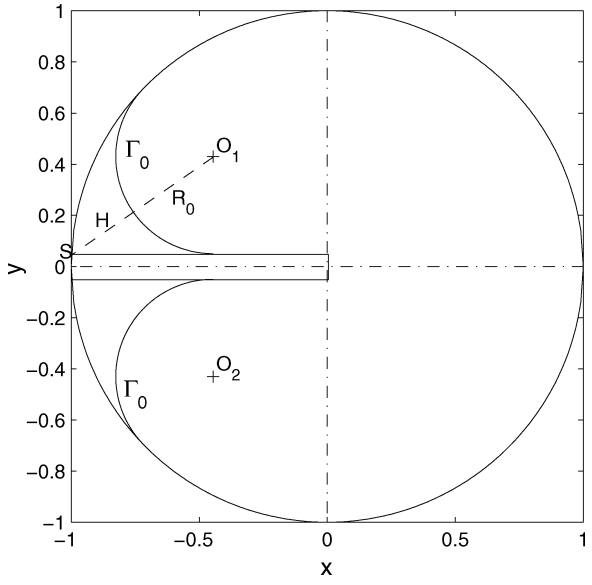

Fig. 9 Location of arc Γ_0 that features the C-singular asymptotic solution surface, $\epsilon = 1.27$ mm, $\delta = 0$, $\gamma = 0$ deg.

zero-gap case. It is not clear whether this variation is caused mainly by the geometric difference or the experimental error. In addition, the increasing difference at large gap size is expected because the larger the gap size, the less the similarity between the geometry in this study and the perfect corners.

The slope m manifests the competition between the capillary and viscous forces. Because one side of the vane is fixed at the center of the tank, an increase of the gap size will not affect the location of the arc Γ_0 shown in Fig. 9. The solid surface area that is in contact with the liquid decreases with the gap size and so do the viscous forces. In addition, the capillary forces may also decrease with the gap size. It is shown by Chen and Collicott[1] that for a small gap such as $\delta = 0.64$ mm, the critical contact angle is 62.8 deg. Most noteworthy is that this critical contact angle is greater than the 46.4-deg critical contact angle for the zero-gap case. But it is not clear whether this is the reason that m increases slightly with gap size when the gap is small. More study needs to be done to understand this behavior.

Effect of the Gap with the Vane Asymmetric to the Wall

Two corners with different angles, one obtuse and the other acute, are formed when the vane is not on a radius of the cylinder. Because the meniscus is connected through the gap, the flow is determined by a combination of the effects from both sides of the vane for any nonzero gap. Menisci near the end of the free fall for different gap sizes are shown in Fig. 10. Results for the meniscus tip location are shown in Fig. 11. For all the non-zero-gap cases, m decreases monotonically with increasing gap size. In addition, m for the zero-gap case at the side with acute corner angle is larger than m with finite δ.

Effect of Obliquity Angle α

Again, one obtuse and one acute angle corner are formed for nonzero obliquity angle α. It is anticipated that the increase of the obtuse angle should slow the flow, whereas the decrease of the acute angle on the other side should speed it up. Results of different α ranging from 0 to 20 deg are shown in Fig. 12. Monotonical increase

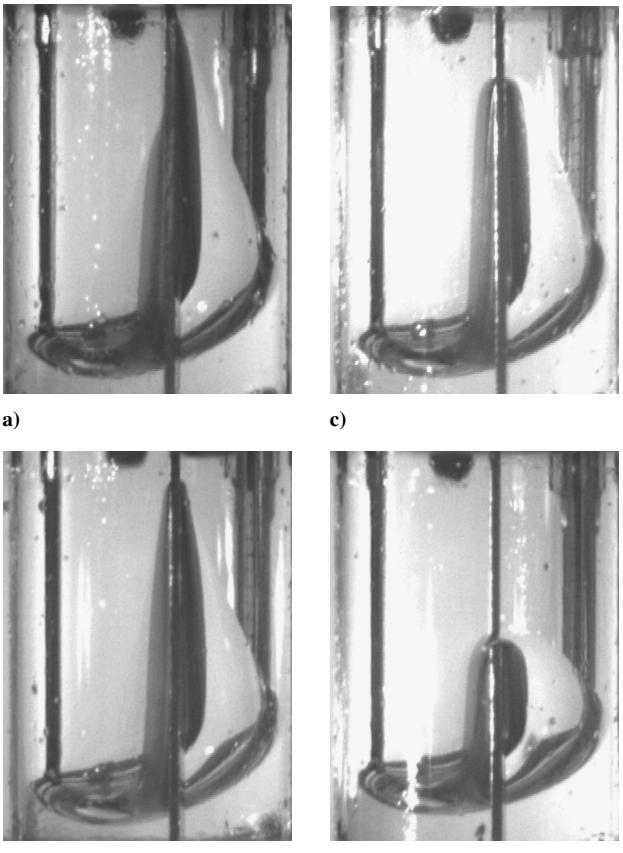

a) **c)**

b) **d)**

Fig. 10 Menisci at about 1.2 s, $\epsilon = 1.27$ mm, $\alpha = 10$ deg, $\nu = 5$ cSt, and differing gap sizes δ: a) 0, b) 0.64, c) 1.27, and d) 2.54 mm.

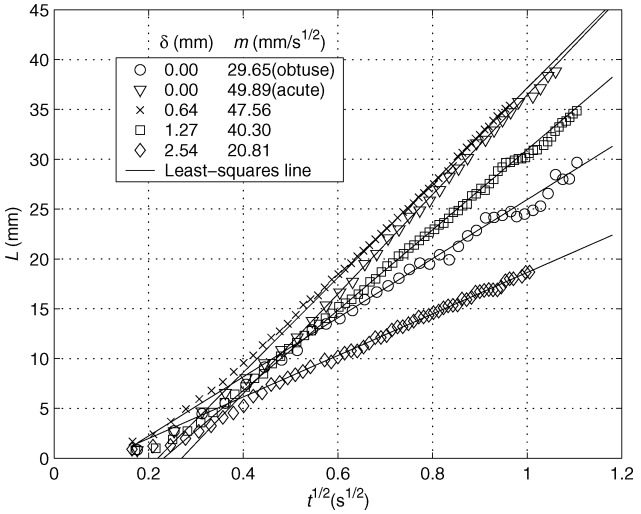

Fig. 11 Meniscus tip location for the vane not normal to the wall, $\epsilon = 1.27$ mm, $\alpha = 10$ deg, $\nu = 5$ cSt.

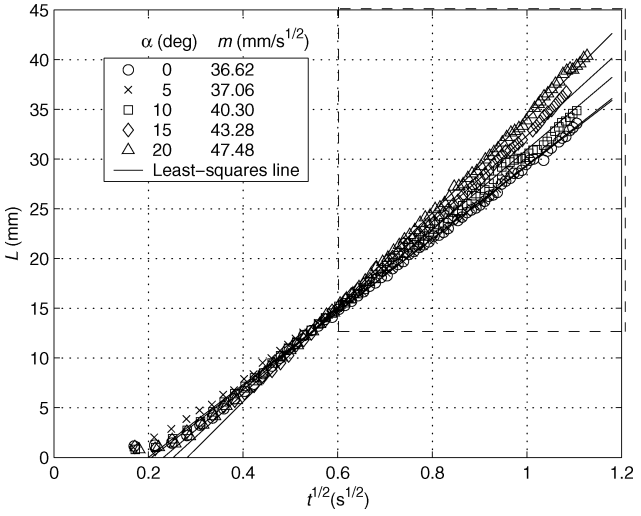

a)

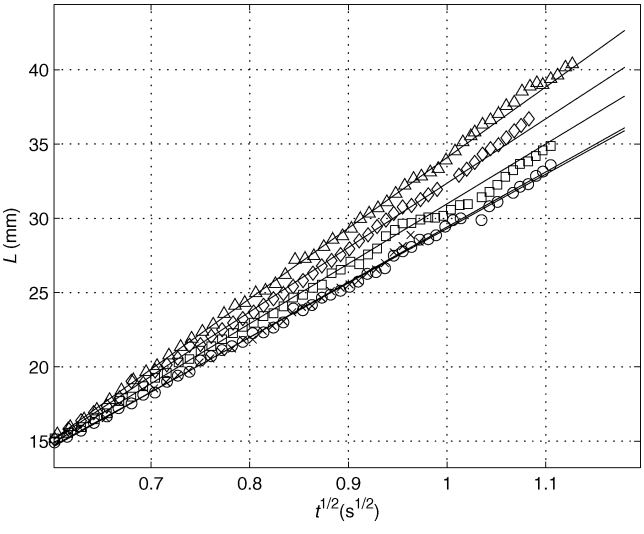

b)

Fig. 12 Results for the effect of obliquity angle: a) meniscus tip location L as a function of $t^{1/2}$ at different angles α; $\epsilon = 1.27$ mm, $\delta = 1.27$ mm, $\nu = 5$ cSt; and b) enlarged view of the region between dashed lines in panel a.

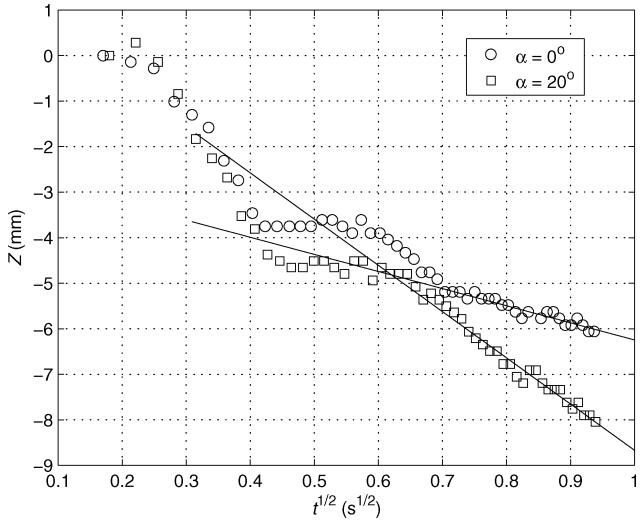

Fig. 13 Interface minimum Z as a function of $t^{1/2}$ at different α, $\delta = 1.27$ mm, $\alpha = 0$ deg, $\nu = 5$ cSt.

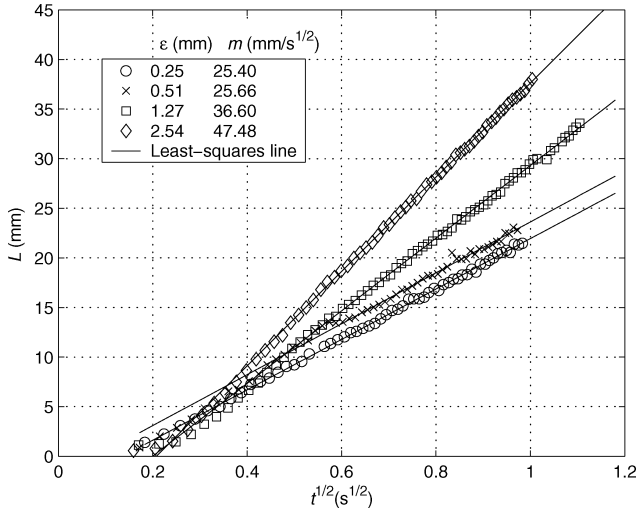

Fig. 14 Meniscus tip location L as a function of $t^{1/2}$ at different ϵ, $\delta = 1.27$ mm, $\alpha = 0$ deg, $\nu = 5$ cSt.

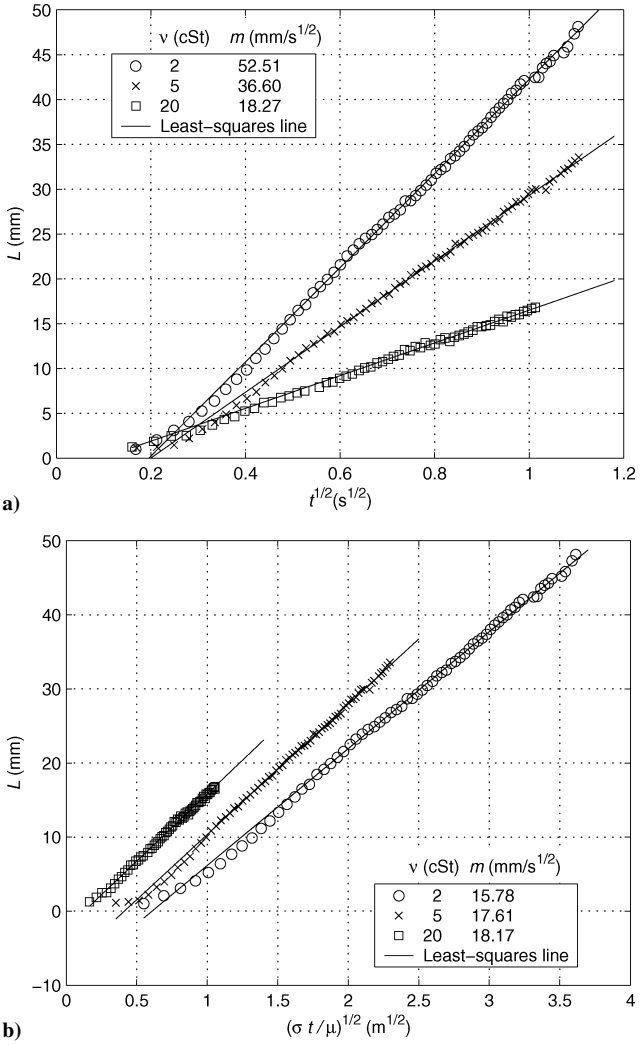

Fig. 15 Meniscus tip location data at different viscosities; $\epsilon = 1.27$ mm, $\delta = 1.27$ mm, $\alpha = 0$ deg: a) L as a function of $t^{1/2}$ and b) L as a function of $(\sigma t/\mu)^{1/2}$.

of m with α can be observed. This means that the increase of the driving forces from the acute corner side is stronger than the loss on the other side. Note also the slight increase in m with α increasing from 0 to 5 deg.

Figure 13 shows the variation of the interface minimum at different α. The least-squares lines reveal that $Z \sim t^{1/2}$ in the Lucas–Washburn regime, which is also found for the flow for interior corners shown by Weislogel.[3] Note that the turning point t_3 marked in Fig. 6b cannot be found unambiguously in the data for $\alpha = 20$ deg.

Effect of the Vane Thickness ϵ

In contrast to holding the vane thickness ϵ constant while increasing the gap size δ, increasing ϵ while keeping δ constant produces an increase in both the viscous and the capillary forces. Fig. 14 shows an increase in m with increasing ϵ. This suggests a greater increase in the capillary forces than in the viscous forces.

Effect of the Viscosity ν

Because the flow in the Lucas–Washburn regime is governed by the competition between the capillary and viscosity forces, it is expected that the tip velocity will decrease when the viscosity of the fluid is increased, provided that the cross-section geometry remains the same. This is evident in Fig. 15a. Furthermore, in Eq. (1), which describes the tip location, $G = \Phi\sigma/\mu$, where Φ is a function of geometric parameters. For the same cross-section geometry, Φ and H are constant values; hence $(\sigma/\mu)^{1/2}$ can be combined with $t^{1/2}$. This treatment produces the results shown in Fig. 15b, where the slopes of the least-squares fitted lines for the three cases vary within 15%. This suggests an analogy between the flow in interior corners and the vane–wall gap geometry. The offset between the different data sets is caused by both experimental error and the difference in the initial inertial response time, defined as $(\rho R^3/\sigma)^{1/2}$, which determines the duration of the first flow regime.

Effect of the Contact Angle γ

Figure 16 shows the effects of different contact angles on the capillary rise. From Weislogel and Lichter[3] it is known that the capillary driving force decreases with increases in the contact angle. As expected, the tip velocity drops with increases in contact angle. Figure 16b shows the measurement of the interface minimum Z. Interface reorientation data of a supercritical case where $\gamma = 51$ deg are included for comparison. Damped oscillations of the interface minimum during the surface reorientation is evident with $\gamma = 51$ deg. With the decrease of the contact angle, the oscillation of the interface is weaker, and thus the inertial forces are weaker compared to the capillary forces. Note that because the different contact angle values were obtained with mixtures of various concentration, both viscosity and surface tension differ slightly between the mixtures.

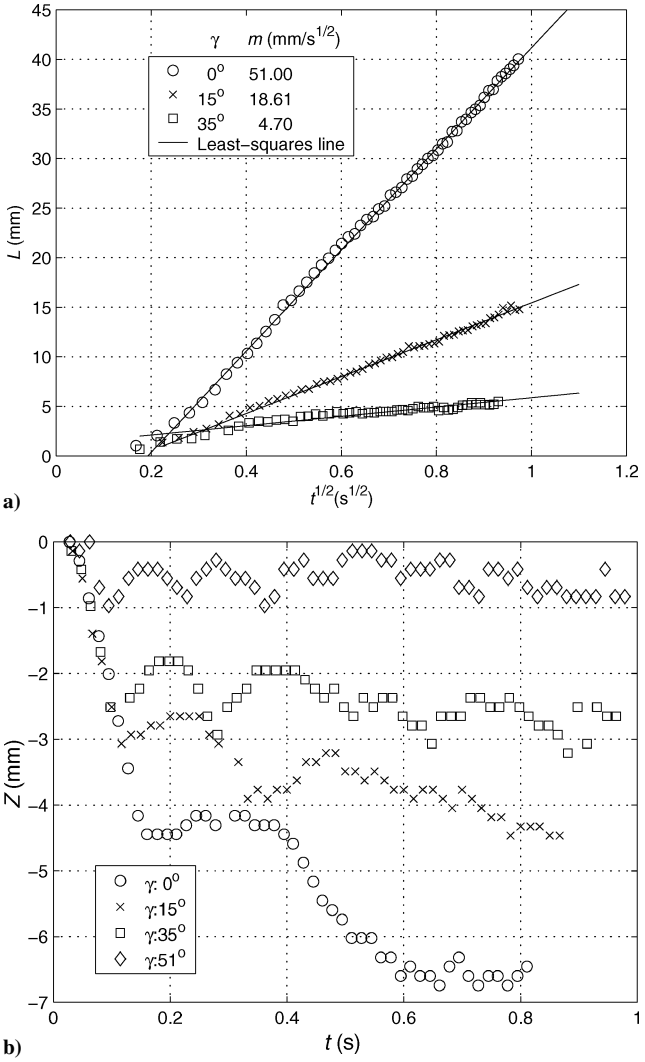

Fig. 16 Capillary rise data at different contact angle; $\epsilon = 1.27$ mm, $\delta = 1.27$ mm, $\alpha = 0$ deg: a) meniscus tip location L as a function of $t^{1/2}$ and b) interface minimum.

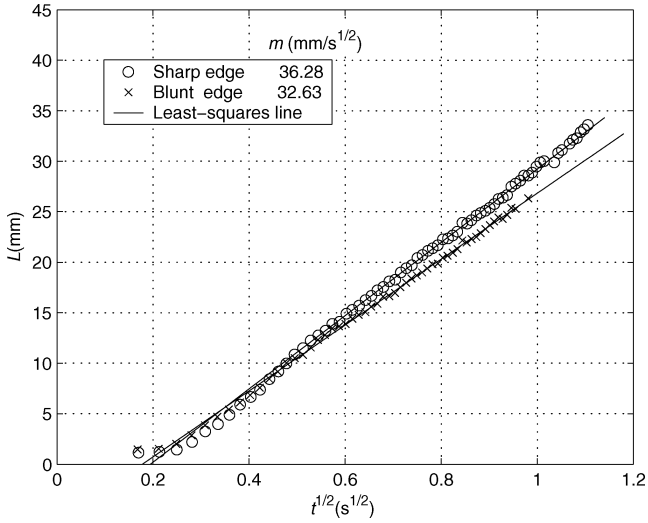

Fig. 17 Meniscus tip location at different vane edge bluntness.

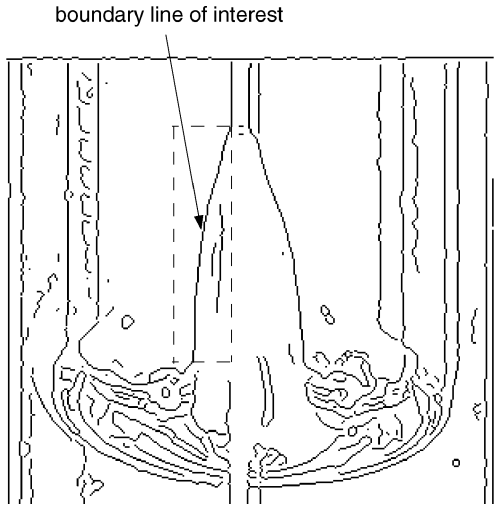

Fig. 18 Image sample after the edge detection treatment.

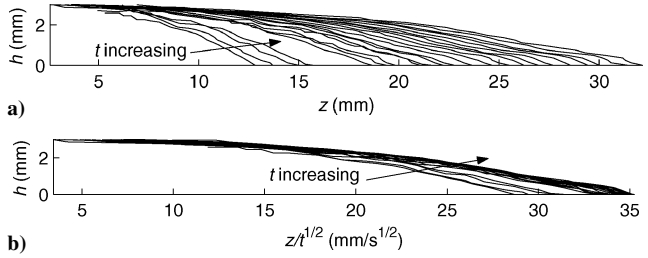

Fig. 19 Representatives of interface profile, t: 0.2–0.83 s, $\epsilon = 1.27$ mm, $\delta = 0.64$ mm: a) h (mm) as a function of z (mm), $t = 0.2$ s for the first trace; and b) h (mm) as a function of $z/t^{0.5}$.

Effect of the Edge Bluntness

In the end, the effect of vane edge bluntness, a typical consequence of manufacturing, is tested. Not only is the effect quantified in the range of known bluntnesses, but the results serve to highlight how the "sharp"-edged results may be affected by bluntness. That is, the vane edges were machined as sharp as feasible, but they cannot be sharp corners in a mathematical sense.

Two vanes were tested, one having nominally sharp edges, as in the cases described, and the other having edges of bluntness close to round, as shown in Fig. 3. The contact line tends to pin on a sharp edge while a rounded edge might slow the tip movement by reducing the pressure gradient along the interface. It turns out that there is as much as 11% reduction in m between the two cases, as shown in Fig. 17.

Interface Profile

Normally, the interface in a plane perpendicular to the flow direction can be assumed to be a construct of a circular arc. Such an arc can be determined if only one point on the arc is located for a known contact angle. As a result, the entire interface can be represented by a profile of the interface in its symmetry plane, which is also the case for the flow in the corners. Weislogel and Lichter[3] have shown the similar behavior of all the traces representing the interface profile when the longitudinal distance z is normalized by $t^{1/2}$.

The geometric configuration in this study makes it impossible to obtain similar data that represent the interface profile appropriately. However, some effort has been made to extract some useful information from the results. From the image data, such as those shown in Fig. 5, one can distinguish a narrow and relatively dark region below the meniscus tip. The evolution of the boundary of this region may shed some light on the interface evolution, provided that the orientation between the camera and the test cell does not vary significantly. Note that this boundary is not the contact line on the wall. Figure 18 shows a sample image after a certain edge-detection treatment. The boundary lines were then extracted from the images out of one drop test and plotted together, as shown in Fig. 19, in which the transverse dimension h is plotted against the streamwise distance z (and rotated 90 deg relative to the drop tower images presented earlier). It is of interest to note that after z is normalized

by $t^{1/2}$, a convergence of the data traces with time can be observed. Such behavior indicates that similarity solutions may also exist for the capillary rise flow problem in the vane–wall gap geometry.

Error Analysis

In the study of capillary flow, the initial condition of the container wall affects the results. Three different initial conditions have been defined by Mumley et al.[17]: dry, prewet–dried, and prewet surfaces. The Purdue drop tower achieves a productive drop rate by eliminating the need to vent the vacuum between drops. For any planned test set, only the very first drop test may achieve a prewet–dried or even dry surface condition if desired. All the rest of the drops have a prewet condition if the time interval between any two consecutive drops is short. It was found that even for those tests, the surface condition depends strongly on the length of the time interval during which the fluid drains back to the liquid bulk and leaves a thin film on the container wall.

As an example, some typical data using silicon oils are shown in Fig. 20. The longest interval is 132 min for "test 1," whereas the shortest one is 10 min for "test 3." The slopes vary by 13% between test 1 and test 3. For tests of the same interval, Fig. 20b shows the original measurement of tip location L and the percentage difference at each moment. The percentage difference can be significant in the early stage of the flow when the magnitude of L is relatively small. Fortunately, the error drops rapidly to within 10% after $t \approx 0.3$ s and 5% after $t \approx 0.5$ s. To create consistency, all of the data with silicon oil as test fluid presented have 10-min intervals between drops.

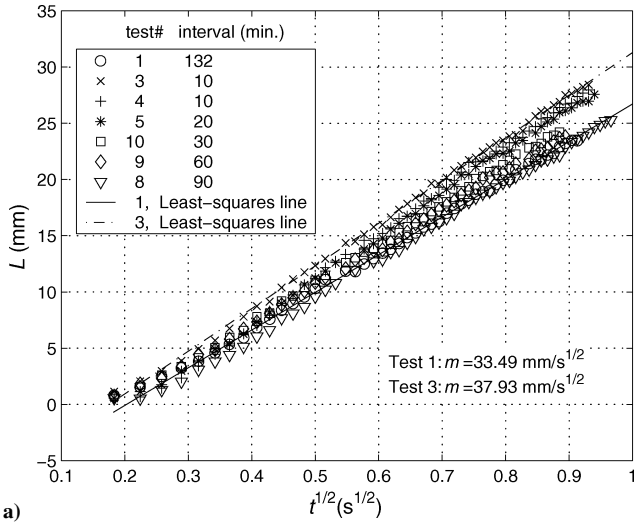

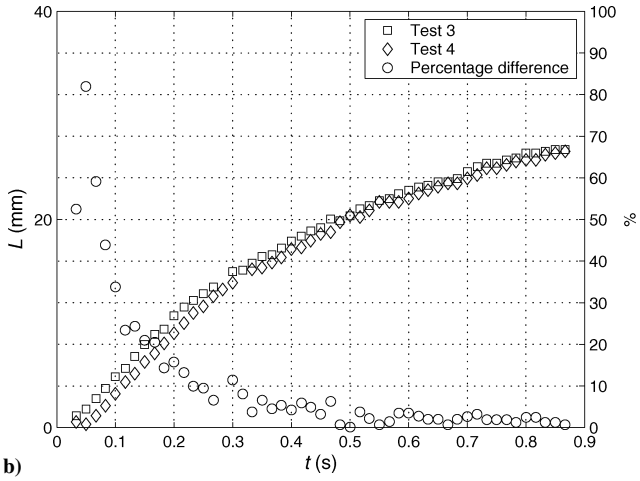

Fig. 20 Effect of initial surface condition on the meniscus tip locations; $\epsilon = 1.27$ mm, $\delta = 1.27$ mm, $\nu = 5$ cSt(PDMS), $\alpha = 0$ deg, $\gamma = 0$ deg: a) data of sequences with different interval and b) data of sequences with the same interval of 10 min.

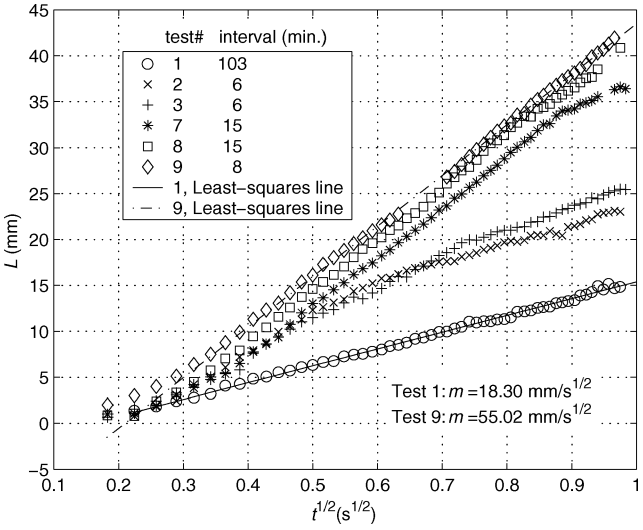

Fig. 21 Effect of initial surface condition on the meniscus tip locations: $\epsilon = 1.52$ mm, $\delta = 1.27$ mm, $\nu = 2.47$ cSt(Eth-H_2O,%70/30), $\alpha = 0$ deg, $\gamma = 15$ deg.

It was observed that the behavior of the mixture of ethanol and distilled water varies much more dramatically with the time interval. Data of a mixture solution with 15-deg contact angle are plotted in Fig. 21. Note that the slope m does not change monotonically with the time interval and that the variation between the maximum and minimum can be nearly 200%. Possible reasons for this behavior might be the random variation of the film thickness left behind by the mixture solution after each drop. As a result, only the data from the first drop are used for all of the tests using the mixture solution.

During the data reduction, a problem has been encountered that concerns the determination of the initial moment when the test cell starts the free fall. In this study, it was determined by initial variation of the meniscus in the images captured. It is almost impossible to identify this moment exactly with the images because there is a time interval between consecutive images. The camera has a standard rate of 30 frames per second. Because it works in an interlaced mode, there is observable variation of information from field to field. This fortunately doubles the framing rate when the two fields are extracted from every single image. Consequently, the image-acquisition rate is doubled to 60 images per second. In this way, the error in determining the initial moment of the free fall of the test cell is less than 17 ms.

Because the camera does not fall in vacuum, it gradually lags behind the test cell due to drag. Another source of error concerns the shift of the test cell in the images of each test. The scale attached to the test cell, the meniscus tip, and the interface minimum are in different planes normal to the axis of the imaging lens. This causes error in the measurement of the tip location. It was examined that this error is within 1.8 mm in the tip measurement and within 0.6 mm in the interface minimum measurement.[13] All of the data presented relating to meniscus tip location L are corrected appropriately, whereas the original interface minimum data are used because no quantitative analysis has been done and the measurement error is much less significant.

Conclusions

Capillary flow in a vane–wall gap geometry has been studied by drop tower experiments. This geometry consists of two corners connected with a gap. Although different flow regimes dominated by inertial force, convective pressure loss, and viscous forces competing against capillary forces have been identified, the research has been focused on the very last one, also known as the Lucas–Washburn regime.

Effects of geometric parameters, contact angle, and fluid viscosity on the flow have been investigated. Dependence of the flow

characteristics on the parameters is mostly nonlinear. It is found that the meniscus tip advance rate drops with the increases in gap size, contact angle, fluid viscosity, and edge bluntness. Increases in the vane thickness and the obliquity angle of the vane will, however, increase the capillary rise rate.

The evolution of the interface is examined approximately with certain relevant data. The collapse of such data after they are normalized by $t^{1/2}$ suggests the existence of similarity solutions for the flow. This requires further investigation.

This work shows that a small gap between a PMD vane and a tank wall can still produce wicking in a manner similar to a solid corner. Specifically, the large time-advance rate scales with the square root of time. Neither small angular misalignment of the vane nor bluntness of the vane edges destroy the wicking necessary for proper PMD performance. The research also verifies the large contact-angle performance of the geometry, thus illustrating suitability for control of a variety of liquids in weightlessness.

Acknowledgment

Purdue University provided graduate support for the first author plus laboratory space and machine shop time. A gift from Lockheed Martin matched by the second author's NSF Career Award (CTS 95-01881) created the drop tower. The authors thank M. Weislogel of Portland State University for many helpful discussions and suggestions.

References

[1]Chen, Y., and Collicott, S. H., "Investigation of the Symmetric Wetting Behavior of Vane–Wall Gaps in Propellant Tanks," *AIAA Journal*, Vol. 42, No. 2, 2004, pp. 305–314.

[2]Chen, Y., and Collicott, S. H., "Investigation of the Wetting Behavior of Asymmetrical Vane–Wall Gap in Propellant Tanks," AIAA Paper 2003-4893, July 2003.

[3]Weislogel, M. M., and Lichter, S., "Capillary Flow in an Interior Corner," *Journal of Fluid Mechanics*, Vol. 373, 1998, pp. 349–378.

[4]Smedley, G., "Preliminary Drop-Tower Experiments on Liquid-Interface Geometry in Partically Filled Containers at Zero Gravity," *Experiments in Fluids*, Vol. 8, No. 6, 1990, pp. 312–318.

[5]Weislogel, M. M., and Ross, H. D., "Surface Reorientation and Settling in Cylinders upon Step Reduction in Gravity," *Microgravity Science and Technology*, Vol. 3, No. 1, 1990, pp. 24–32.

[6]Jaekle, D. E., "Propellant Management Device Conceptual Design and Analysis: Vanes," AIAA Paper 91-2172, June 1991.

[7]Stange, M., Dreyer, M., and Rath, H.-J., "Capillary Driven Flow in Circular Cylindrical Tubes," *Physics of Fluids*, Vol. 15, No. 9, 2003, pp. 2587–2601.

[8]Ransohoff, T. C., and Radke, C. J., "Laminar Flow of a Wetting Liquid Along the Corners of a Predominantly Gas-Occupied Noncircular Pore," *Journal of Colloid and Interface Science*, Vol. 121, No. 2, 1988, pp. 392–401.

[9]Dong, M., and Chatzis, I., "The Imbibition and Flow of a Wetting Liquid Along the Corners of a Square Capillary Tube," *Journal of Colloid and Interface Science*, Vol. 172, No. 2, 1995, pp. 278–288.

[10]Dreyer, M., Delgado, A., and Rath, H.-J., "Fluid Motion in Capillary Vanes Under Reduced Gravity," *Microgravity Science and Technology*, Vol. 5, No. 4, 1993, pp. 203–210.

[11]Dreyer, M., Delgado, A., and Rath, H.-J., "Capillary Rise of Liquid Between Parallel Plates Under Microgravity," *Journal of Colloid and Interface Science*, Vol. 163, No. 1, 1994, pp. 158–168.

[12]Chen, Y., and Collicott, S. H., "A New Design of Drop Tower to Study Uncertainties in Zero-Gravity Fluid Mechanics," AIAA Paper 2001-0609, Jan. 2001.

[13]Chen, Y., "A Study of Capillary Flow in a Vane–Wall Gap in Zero Gravity," Ph.D. Dissertation, School of Aeronautics and Astronautics, Purdue Univ., West Lafayette, IN, Aug. 2003.

[14]Siegert, C. E., Petrash, D. A., and Otto, E. W., "Time Response of Liquid–Vapor Interface After Entering Weightlessness," NASA TN D-2458, 1964.

[15]de Lazzer, A., Langbein, D., Dreyer, M., and Rath, H.-J., "Mean Curvature of Liquid Surfaces in Cylindrical Containers of Arbitrary Cross-Section," *Microgravity Science and Technology*, Vol. 9, No. 3, 1996, pp. 208–219.

[16]Finn, R., and Neel, R. W., "C-Singular Solutions of the Capillary Problem," *Journal für die Reine und Angewandte Mathematik*, Vol. 512, July 1999, pp. 1–25.

[17]Mumley, T. E., Radke, C. J., and Williams, M. C., "Kinetics of Liquid/Liquid Capillary Rise. I. Experimental Observations," *Journal of Colloid and Interface Science*, Vol. 109, No. 2, 1986, pp. 398–412.

S. Aggarwal
Associate Editor